Contributions of Amino Acid Side Chains to the Kinetics and Thermodynamics of the Bivalent Binding of Protein L to Ig κ Light Chain†

Henrik G. Svensson,*,‡ William J. Wedemeyer,§ Jennifer L. Ekstrom,# David R. Callender,§ Tanja Kortemme,§ David E. Kim,§ Ulf Sjöbring,‡ and David Baker§

Lund University, BMC B14, Tornavägen 10, S-22184 Lund, Sweden, Box 357350, University of Washington, Seattle, Washington 98195-7350 USA, and Department of Biochemistry and Biophysics, University of California San Francisco, San Francisco, California 94143-0448 USA

Received May 23, 2003; Revised Manuscript Received September 25, 2003

ABSTRACT: Protein L is a bacterial surface protein with 4−5 immunoglobulin (Ig)-binding domains (B1−B5), each of which appears to have two binding sites for Ig, corresponding to the two edges of its β-sheet. To verify these sites biochemically and to probe their relative contributions to the protein L−Ig κ light chain (κ) interaction, we compared the binding of PLW (the Y47W mutant of the B1 domain) to that of mutants designed to disrupt binding to sites 1 and 2, using gel filtration, BIAcore surface plasmon resonance, fluorescence titration, and solid-phase radioimmunoassays. Gel filtration experiments show that PLW binds κ both in 1:1 complexes and multivalently, consistent with two binding sites. Covalent dimers of the A20C and V51C mutants of PLW were prepared to eliminate site 1 and site 2 binding, respectively; both the A20C and V51C dimers bind κ in 1:1 complexes and multivalently, indicating that neither site 1 nor site 2 is solely responsible for κ binding. The A20R mutant was designed computationally to eliminate site 1 binding while preserving site 2 binding; consistent with this design, the A20R mutant binds κ in 1:1 complexes but not multivalently. To probe the contributions of amino acid side chains to binding, we prepared 75 point mutants spanning nearly every residue of PLW; BIAcore studies of these mutants revealed two binding-energy "hot spots" consistent with sites 1 and 2. These data indicate that PLW binds κ at both sites with similar affinities (high nanomolar), with the strongest contributions to the binding energy from Tyr34 (site 2) and Tyr36 (site 1). Compared to other protein−protein complexes, the binding is insensitive to amino acid substitutions at these sites, consistent with the large number of main chain interactions relative to side chain interactions. The strong binding of protein L to Ig κ light chains of various species may result from the ambidextrous binding of the B1−B5 domains and the unimportance of specific side chain interactions.

Protein L is an immunoglobulin (Ig)[1]-binding protein found on the surface of some strains of the anaerobic bacterium *Peptostreptococcus magnus* (*1*). Protein L correlates with the virulence of such bacteria (*2*, *3*) and can induce histamine release from human basophils and mast cells by binding and cross-linking IgE on the surface of these cells (*4*, *5*). Protein L from *P. magnus* strain 312 has five homologous Ig-binding domains (denoted as B1−B5) of 72−76 residues each (*6*). Although the initial residues of B1 are disordered (*7*), its C-terminal 62 residues form a very stable domain (*8*) ($T_m \approx 70$ °C), consisting of a single α-helix roughly parallel to a four-stranded β-sheet with an unusual, ubiquitin-like topology 2−1−4−3 (*9*, *10*) (Figure 1). This structure closely resembles the structure of the corresponding domain in protein G from group C and G streptococci (*11*−*13*), although there is no detectable sequence homology and the two domains differ in their binding specificity. Whereas the Ig-binding domains in protein G and in protein A from *Staphylococcus aureus* (*14*) bind to only Ig heavy chains, the protein L domains bind to only Ig κ light chains (κ) from a variety of mammalian species (*1*, *15*, *16*). Specifically, protein L binds to the framework region of the variable domain of the $V_{\kappa I}$, $V_{\kappa III}$, and $V_{\kappa IV}$ subgroups but does not

† This work was supported by grants from the Swedish Medical Research Council (project #9926), the Swedish Society for Medical Research, the Royal Physiographic Society in Lund, the Kock, Wiberg, and Österlund Foundations, King Gustav V's 80-year Foundation, and the Howard Hughes Medical Institute. T.K. was supported by the Human Frontier Science Program and the European Molecular Biology Organisation.

* To whom correspondence should be addressed. Present address: Division of Cell Biology and Immunology, University of Dundee, Dundee, DD1 5EH, UK. Telephone: +44−1382−345096. Fax: +44−1382−345783.

‡ Lund University.

§ University of Washington.

University of California San Francisco.

[1] Abbreviations: PpL, a generic immunoglobulin-binding domain of protein L; PLW, the Y47W mutant of the B1 domain of protein L; IgG and IgE, immunoglobulins G and E; V_L and C_L, the variable and constant domains of Ig light chain; V_H and C_H, the variable and constant domains of Ig heavy chain; V_κ, the variable domain of Ig κ light chain; SPR, surface plasmon resonance; SPRIA, solid-phase radioimmunoassay; PBS, phosphate-buffered saline.

10.1021/bi034873s CCC: $27.50
Published on Web 02/13/2004

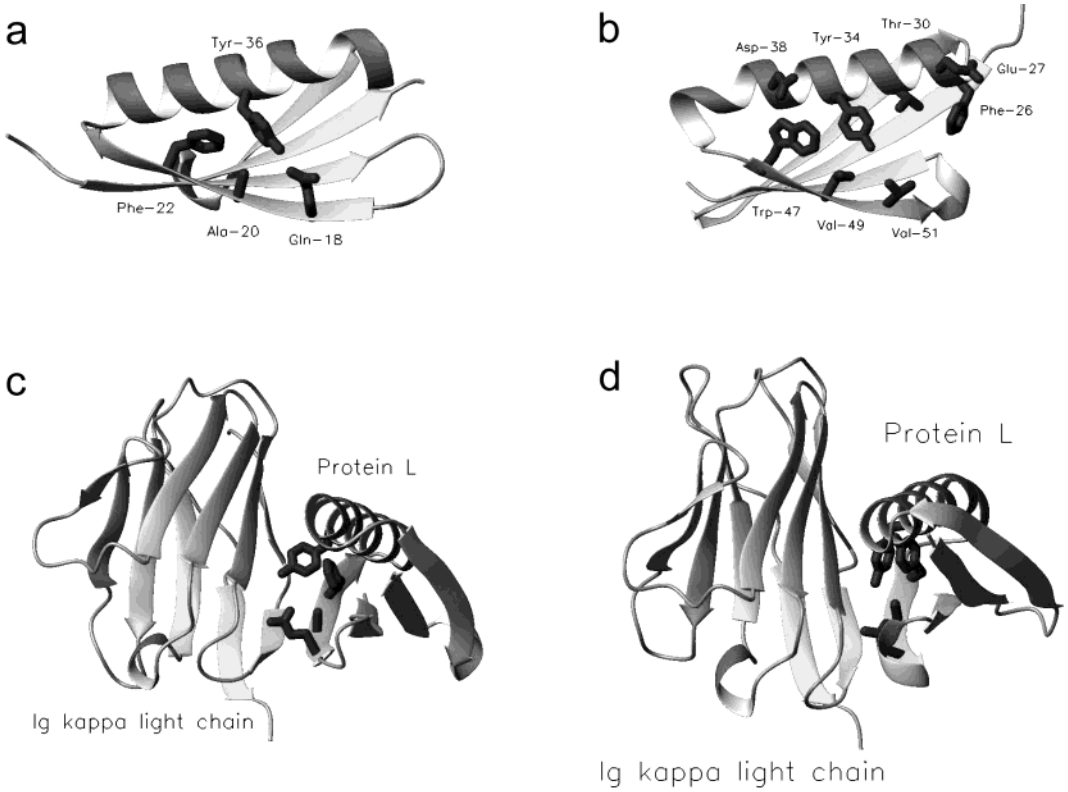

FIGURE 1: Ribbon diagrams of the two binding sites on the B1 domain of protein L alone and in complex with Ig κ light chain, taken from a high-resolution X-ray crystal structures (PDB accession code 1hz5 for a and b and 1hez for c and d). (a) Site 1; the positions of Gln-18, Ala-20, Phe-22, and Tyr-36 are indicated. (b) Site 2; the positions of Phe-26, Glu-27, Thr-30, Tyr-34, Asp-38, Trp-47, Val-49, and Val-51 are indicated. (c) Site 1 on protein L binds to the second β-strand of the variable domain of Ig κ light chain with *antiparallel* β-strands. (d) Site 2 on protein L binds to the same site on Ig κ light chain, but with *parallel* β-strands. The figures were created using the program MOLMOL (*45*).

appear to bind to heavy chains, Ig λ light chains, the C_L domains of κ, or the variable domain of the $V_{\kappa II}$ subgroup (*17*).

In recent X-ray structures (*18*−*20*), a single site on the κ was observed to bind at two separate sites on the B1 domain of protein L, denoted here as site 1 and site 2 (Figure 1a,b, respectively). At site 1, the second β-strand of B1 binds antiparallel to the second β-strand of the V_κ domain (Figure 1c), whereas, at site 2, the third β-strand of B1 binds parallel to the same β-strand of the V_κ domain (Figure 1d). Previous biochemical studies, however, have detected only a single binding site on PpL (*6*, *21*), consistent with the absence of precipitation between the two isolated domains (*6*) and with NMR studies that detected binding at site 1 but no definitive evidence for binding to site 2 (*19*, *22*). A more recent binding study (*23*) found that the site 1 mutation Y36F lowers the affinity 50-fold (from roughly 100 nM to 3 μM), suggesting that binding occurs predominantly at site 1 on B1. These observations suggest that the site 2 binding may be an artifact of crystallization.

To verify these sites biochemically and to probe their relative contributions to protein L−κ binding in solution, we compared the binding of PLW (the Y47W mutant of the B1 domain) to that of mutants designed to disrupt binding to sites 1 and 2, using gel filtration, BIAcore surface plasmon resonance, fluorescence titration, and solid-phase radioimmunoassays. We find that both sites contribute to binding in solution. Specifically, the A20C and V51C covalent dimers bind multivalently (despite the respective disruption of sites 1 and 2), while the A20R mutant (designed to eliminate site 1 binding) forms only 1:1 complexes with κ in solution. We further obtain a detailed map of side chain contributions in both sites by characterizing the effects of 75 mutations in PLW on both the kinetics and thermodynamics of κ binding. BIAcore studies of these mutants revealed two binding-energy "hot spots" consistent with sites 1 and 2.

MATERIALS AND METHODS

Materials. Most of the 75 PLW variants have been described previously (*24*); the additional site-specific mutations were made with the QuikChange site-directed mutagenesis kit (Stratagene) using the protocol suggested by the manufacturer. A pET15b-derived construct expressing PLW (*25*) was used as a template. All mutations were verified by DNA sequencing using the ABI Prism BigDye Terminator Cycle Sequencing Ready Reaction kit (PE Applied Biosystems). Expression and purification of PLW and its mutants were carried out as described previously (*8*). Human polyclonal IgG was purchased from Pierce and used without further purification. The human Ig κ light chain 4479 was a generous gift from Dr. Lars Björck of Lund University in Sweden.

Gel Filtration Experiments. Varying concentrations of PLW (or a mutant thereof) and Ig κ light chain were run on two different Pharmacia Biotech Superdex 75 HR 10/30 analytical gel filtration columns. The molecular weight standards used on column 1 were aprotinin, ribonuclease A, chymotrypsinogen, ovalbumin, and albumin, whereas the molecular weight standards used on column 2 were aprotinin,

cytochrome C, carbonic anhydrase, bovine serum albumin, and blue dextran (to determine the void volume). The buffer was the same PBS as used in the SPR experiments, described below. The protein concentration was monitored simultaneously at 215, 280, and 310 nm for column 1 and at 280 nm for column 2.

Surface Plasmon Resonance (SPR) Experiments. SPR experiments were carried out using BIAcore 2000 and BIAcore X optical biosensors (Biacore, Inc., Uppsala, Sweden). Purified Ig κ light chains were resuspended at 0.5 μM in 10 mM sodium acetate pH 3.4 and immobilized to CM-5 sensor chips using standard amino-coupling chemistry following the protocol recommended by the manufacturer (www.biacore.com). Binding experiments were carried out using PBS (1.4 mM KH_2PO_4, 10.1 mM Na_2HPO_4, 137 mM NaCl, and 2.7 mM KCl) containing 50 μM EDTA and 0.005% Tween-20 as the running buffer and 50 mM HCl as the regeneration buffer. All experiments were carried out at a flow rate of 40 μL/min to avoid mass transport effects, and were carried out using 6−7 different concentrations of the analyte. The standard method of "double referencing" (*26*) was used to eliminate artifacts due to the flow chambers. Control experiments were carried out in which PLW was passed over a chip to which Ig λ light chain had been immobilized; no binding was detected, indicating that the sensorgrams are reporting on *specific* binding of PLW and Ig κ light chain.

In standard SPR experiments, PLW or one of its mutants at various concentrations was passed over the Ig κ light chain-decorated BIAcore chip for 150 s, followed by a dissociation phase of 300−900 s in which no PLW was present in the running solution. The amplitudes and rates of the association and dissociation phases were fit using the Kaleidagraph program (Synergy Software, Reading, PA). The data were fit to successively more exponentials until no significant improvement in χ^2 could be obtained; the association data fit well to a single exponential and a constant, whereas the dissociation data fit well to two exponentials and a constant.

In the SPR titration experiments, PLW or one of its mutants was passed over the BIAcore chip at various concentrations for 600 s, followed by a dissociation phase monitored for 600 s. The long association time was used to ensure that the association had fully equilibrated. The amplitudes of the three dissociation phases were obtained as in the standard SPR experiments, and were plotted versus the concentration of PLW used in the *association* phase.

In the time-lapse SPR experiments, PLW or one of its mutants was passed over the BIAcore chip at various concentrations for various association times *t*, followed by a dissociation phase monitored for 500 s. Fitting of the three dissociation phases was carried out as in the standard SPR experiment. The amplitudes of the dissociation phases were then plotted as a function of the initial *association* time *t*.

Fluorescence Titration. Equilibrium fluorescence measurements were carried out in a Spex Fluorolog 2 spectrofluorimeter; excitation was at 280 nm and emission was measured at 335 nm. All measurements were carried out in 50 mM phosphate with 500 mM NaI. For each measurement, a 0.5 or 0.9 μM solution of Ig κ light chain was mixed with various concentrations of the F22W mutant of PLW and allowed to incubate for at least 15 min prior to measurements. The F22W mutant was used since this was the only mutant that upon binding had a large enough change in fluorescence to enable affinity calculations.

Solid-Phase Radioimmunoassay (SPRIA). The wells of microtiter plates (Microtest III, Becton-Dickinson) were coated with 0.1 nmol of Ig κ light chains in 100 μL of PBS at 4 °C for 18 h. The wells were blocked with PBS buffer containing 0.25% gelatin and 0.25% Tween-20 for 4 h at room temperature, after which the wells were washed four times with the blocking buffer. ^{125}I-labeled PLW and different concentrations of unlabeled PLW (or a mutant thereof) were mixed in a total volume of 100 μL of blocking buffer and added to the wells. After 4 h of incubation at room temperature, the wells were washed four times with blocking buffer and the radioactivity was measured using a gamma counter. All experiments were carried out three times.

Computational Design of PLW Variants to Restrict V_κ Binding to a Single Site. New mutants were designed to significantly destabilize the binding of PLW at sites 1 and 2, respectively. A protein interface design program (*27*) was used to evaluate the effect of mutating residues Q18, A20, F22, Y36 of site 1 on PLW and residues E27, A31, Y34, V51, and G55 of site 2 on PLW in disrupting the PLW−V_κ complex. Residues located in each binding site were computationally replaced by large side chains (K, R, W, and Y). For each binding site in turn, all possible combinations of these amino acids at each position (including the wild-type residue) were calculated, while allowing conformational changes in the neighboring side chains to accommodate the various mutations. Whereas the polypeptide backbones of the interacting proteins were held fixed, the side chain conformations were allowed to vary and were represented as rotamers during the calculation. The free energy changes $\Delta\Delta G$ in the complex and in the isolated molecules were estimated using an energy function composed mainly of van der Waals packing interactions, an implicit solvation model, hydrogen bonding, and statistical terms representing amino acid-dependent conformational preferences (*27*, *28*). The best complexes were then selected based on the degree to which their mutation(s) destabilized the target binding site *without* destabilizing the isolated PLW molecule. This protocol identified A20R as particularly disruptive to site 1 binding, and the V51W/G55R double mutation as particularly disruptive to site 2 binding. These predictions were borne out by the experimental data, although the structural interpretation of the V51W/G55R mutation remains uncertain, due to the possibility of dimer formation.

Computational Alanine Scanning of PL Binding to Ig κ Light Chain. Starting from the crystal structure of the PLW−Ig κ light chain complex (*18*), each nonalanyl, nonglycyl residue on PLW was replaced computationally by alanine. The effect of each mutation on the free energy was evaluated for the complex ($\Delta G_{complex}$) as well as the unbound partners, PLW (ΔG_{PLW}) and Ig κ light chain (ΔG_κ) (*27*). The change in binding free energy upon alanine mutation ($\Delta\Delta G_{bind}$; Table 3) was computed as

$$\Delta\Delta G_{bind} = \Delta G_{complex} - \Delta G_{PLW} - \Delta G_\kappa$$

RESULTS AND DISCUSSION

Disruption of Sites 1 and 2 by Disulfide Dimerization and Computational Redesign. To establish that neither site 1 nor 2 is solely responsible for PLW−κ binding, we sought to

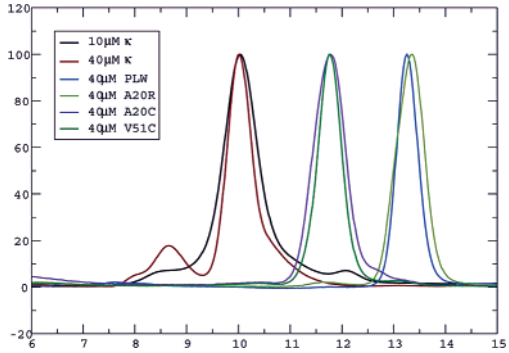

FIGURE 2: Gel filtration experiments on isolated Ig κ light chain, PLW and its mutants A20R, A20C, and V51C. The two peaks at the far right represent the elution profiles of PLW and A20R (blue and green curves, respectively), and are consistent with monomeric species. The middle two peaks represent the elution profiles of the A20C and V51C mutants (magenta and dark green, respectively) and are consistent with dimeric species. Finally, the two peaks at the far left represent the elution profiles of Ig κ light chain at 10 and 40 μM (black and red curves, respectively); the major peak in both cases represents the monomeric Ig κ light chain species, while the minor red peak represents the dimeric Ig κ light chain species.

eliminate binding at each site. We prepared two different covalent dimers by the mutations A20C and V51C; since these residues occupy the center of the sites 1 and 2 (Figure 1), covalent dimerization should eliminate binding to the respective binding sites. Nevertheless, both dimers should be able to form high molecular weight aggregates with κ, since each dimer of V51C and A20C should have two functional binding sites (sites 1 and 2, respectively). We also sought to eliminate the binding to a particular site without dimerization. A successful computational protein−protein interface redesign protocol (*27*, *29*) was used to identify mutations likely to disrupt the binding of sites 1 and 2, while retaining the overall stability of the protein (see Methods). This protocol identified the A20R mutation as particularly disruptive of site 1, and the double mutation V51W/G55R as particularly disruptive of site 2. These two mutants were expressed and purified. As described below, the A20R mutations does disrupt site 1 binding while preserving site 2 binding. However, the V51W/G55R results could not be readily interpreted, due to dimerization.

Gel Filtration Analysis. To determine whether protein L can bind two κ chains in solution, we used gel filtration chromatography to characterize PLW−κ complexes. We cross-checked our results by running the mixtures over two separate Superdex 75 HR 10/30 analytical gel filtration columns (Pharmacia). The results were consistent between both sets of experiments.

At 40 μM concentration, PLW and its three mutants V51C, A20C, and A20R elute as single peaks (Figure 2); the estimated molecular weights of the A20C and V51C mutants are double those of the wild-type protein and A20R mutant, with no discernible peaks at the monomer molecular weight. Therefore, it is reasonable to conclude that the A20C and V51C mutants have indeed formed covalent dimers. Similarly, at 40 μM concentration, the κ chain elutes as two peaks, a major peak and a minor peak at twice the molecular weight of the major peak (Figure 2, red curve). We assign these peaks to the monomeric and dimeric forms of κ, which were also observed using MALDI mass spectroscopy (data not shown); κ are known to form dimers (*30*−*32*) with a K_d of roughly 1 μM (*33*). At 10 μM concentration, the κ dimer peak is much reduced (Figure 2, black curve), indicating that the dimers are noncovalent.

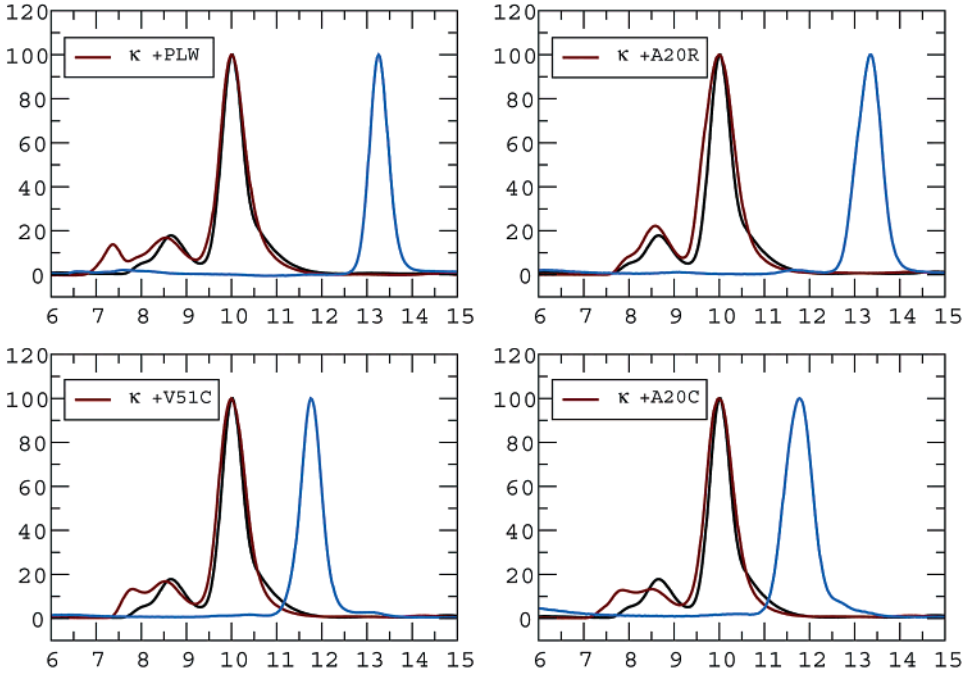

FIGURE 3: Gel filtration experiments on PLW and its mutants A20R, A20C, and V51C in the presence of excess Ig κ light chain. The black and blue curves represent the isolated κ and PLW/mutant elution profiles, respectively (cf. Figure 3), whereas the red curve represents the elution profile for a mixture of 40 μM Ig κ light chain with 10 μM PLW (or its mutants). In all four cases, the monomeric PLW/mutant peak disappears in the presence of excess Ig κ light chain, presumably forming complexes with the Ig κ light chain; a small shift in the Ig κ light chain monomer and dimer peaks toward heavier molecular weights is observed. At the same time, a high-molecular-weight complex is observed for PLW, A20C, and V51C, but not for A20R. This is consistent with our model that the first three proteins can bind bivalently, whereas the fourth cannot. Presumably, the Ig κ light chain can bind PLW multivalently by forming dimers, or possibly through a second (low-affinity) binding site.

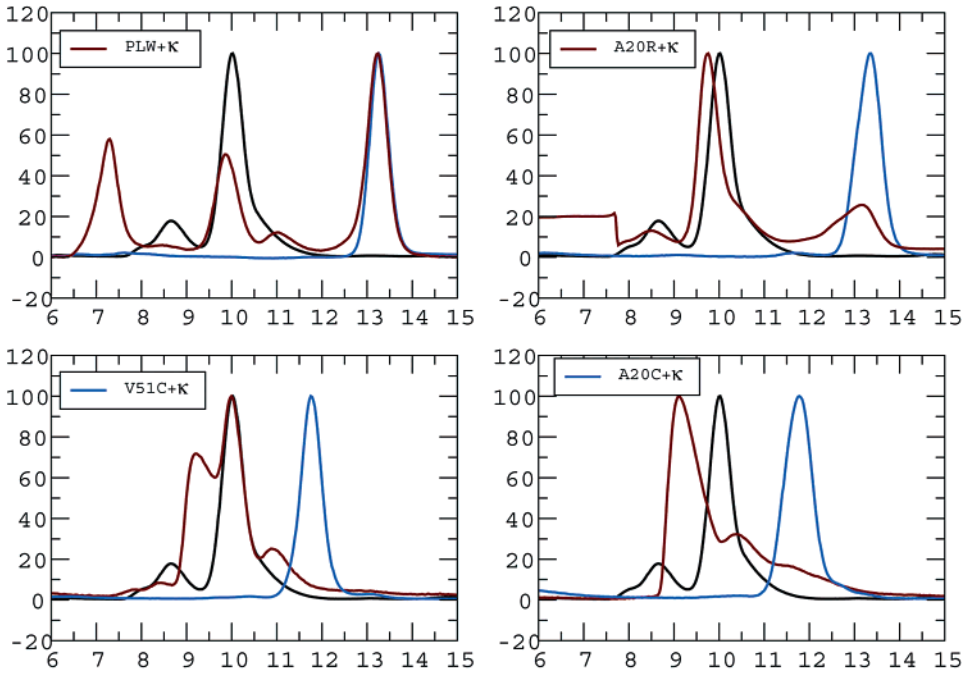

FIGURE 4: Gel filtration experiments on Ig κ light chain in the presence of excess PLW or its mutants A20R, A20C, and V51C. Again, the black and blue curves represent the isolated Ig κ light chain and PLW/mutant elution profiles, respectively (cf. Figure 3), whereas the red curve represents the elution profile for a mixture of 10 μM Ig κ light chain with 40 μM PLW (or its mutants). In all four cases, a 1:1 complex with the Ig κ light chain is apparent. A high-molecular-weight complex is present in the elution profile for PLW, but not in those of its three mutants, possibly reflecting a second (low-affinity) binding site for PLW on the Ig κ light chain.

Chromatography of a solution containing κ in a 4-fold excess over PLW (40:10 μM, respectively) yielded three discernible peaks corresponding to monomeric κ, PLW bound to dimeric κ and large complexes running in the void volume of the column; the peak corresponding to isolated PLW was completely absent (Figure 3). The appearance of large-molecular-weight complexes indicate that PLW is binding multivalently to κ. Similar elution profiles are observed for the V51C and A20C covalent dimers (Figure 3), suggesting that they too can bind to κ multivalently. By contrast, no such complexes are observed for the A20R mutant, although A20R does bind κ in a 1:1 complex (Figure 3), consistent with our design to eliminate the bivalent binding but retain site 2 binding.

Conversely, chromatography of a solution containing the A20R, A20C, or V51C mutant in a 4-fold excess over κ (again 40:10 μM, respectively) yielded three peaks that may be assigned to the unbound mutant, and the mutant bound to monomeric and dimeric κ (Figure 4). A fourth peak of molecular weight between the PLW mutant and monomeric κ can be discerned in some cases, and may correspond to an impurity, e.g., a degraded variant of κ incapable of binding PLW. Finally, wild-type PLW appears capable of forming high-molecular-weight complexes even in the presence of excess PLW; this may signal a second, low-affinity binding site on κ, since the κ dimer is poorly populated at 10 μM κ concentration. Most importantly, these experiments show that all three PLW mutants are capable of binding κ, despite the disruptions of site 1 and 2.

Three SPR Dissociation Phases. To probe the kinetics and thermodynamics of binding, and to investigate the contributions of amino acid side chains in protein L to the interaction with κ, we used surface plasmon resonance to study the binding of PLW and 75 single mutants (60 to alanine) that span nearly every residue of the protein.

The possibility of multivalent binding of protein L and κ suggests that the binding kinetics of κ and PLW will be complex (i.e., multiexponential), as was indeed observed. PLW dissociates from κ immobilized to the BIAcore chip in three phases (Figure 5a,b), denoted here as the fast phase, the slow phase, and the very slow phase. The fast and slow dissociation phases are exponential, with rates of approximately 0.087 and 0.0063 s^{-1}, respectively, under our conditions (Table 1); the rates are independent of the association time and of the concentration of PLW flowing over the chip during association. The fast dissociation rate agrees with that measured in earlier fluorescence experiments (*21*). By contrast, the very slow dissociation phase is nonexponential, and occurs on a time scale of roughly hours (Figure 5b). The nonexponential character of this phase could be partly due to contamination by baseline drift that cannot be removed by double-referencing (*26*). The 75 PLW mutants likewise exhibit triphasic dissociation from immobilized κ, with fast and slow rates (Table 1) that generally agree with those of PLW. Three phases with similar rates are also obtained when PLW is passed over a chip decorated with complete IgG (Figure 5c). The dissociation of κ from immobilized PLW likewise exhibits fast, slow, and very slow exponential phases with roughly similar rates (Figure 5d). These phases must correspond to *specific* binding, since no such phase is observed with Ig λ light chains (Figure 5e), consistent with previous studies (*6*).

The gel filtration experiments and X-ray crystallography suggest that the kinetic complexity seen could be caused by multivalent binding. Such kinetics are hard to analyze by global modeling since there are many possible species and a very large number of parameters describing their inter-

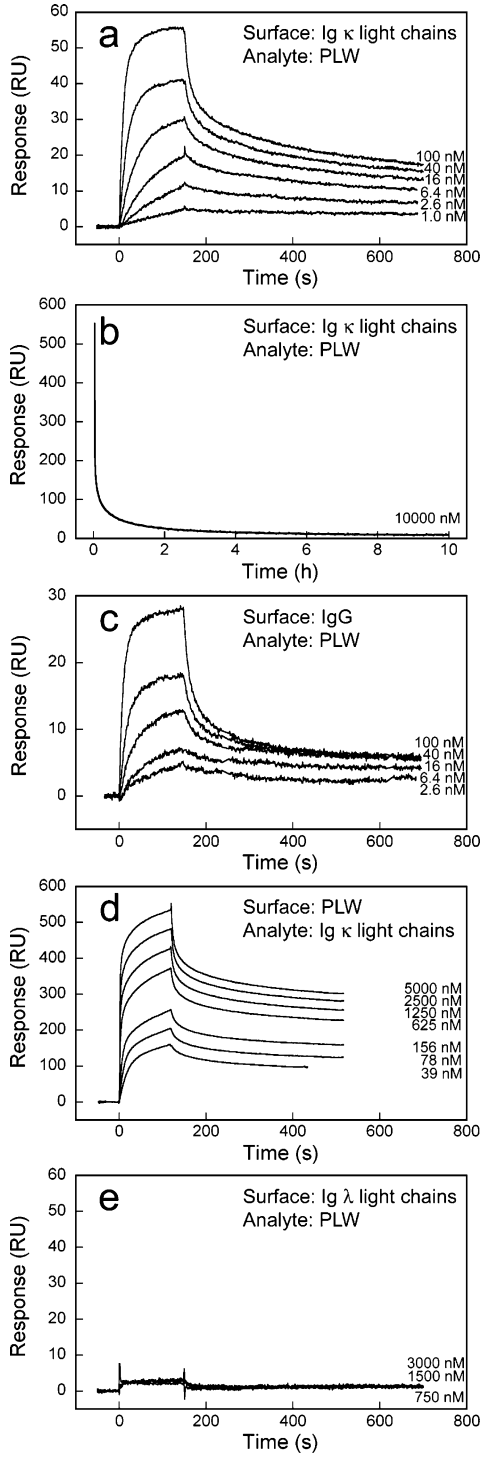

FIGURE 5: (a) Typical SPR sensorgrams for the association of PLW to κ coupled to the BIAcore chip. The dissociation phase is triphasic. The fast and slow apparent dissociation rates differ 10-fold (being 0.087 and 0.0063 s^{-1}, respectively), while the very slow dissociation rate cannot be measured reliably. (b) Dissociation of PLW from immobilized Ig κ light chains measured over a very long time. The very slow phase of dissociation cannot be fit to a single exponential. (c) Typical SPR sensorgrams for the association of PLW to intact IgG immobilized on the chip. (d) Typical SPR sensorgrams for the reversed experiments, in which PLW is coupled to the chip and Ig κ light chain is in the flowing solution. (e) SPR sensorgrams for the association of PLW to Ig λ light chains immobilized on the chip; no specific binding is detected. Immobilization levels were (a) 750 RU Ig κ light chains, (b) 2970 RU Ig κ light chains, (c) 5030 RU polyclonal IgG, (d) 504 RU PLW, and (e) 5550 RU Ig λ light chains.

conversion (for example, for a bivalent complex, the model has to allow for dissociation and reassociation at different rates depending on the occupancy of the other site). We instead present a more qualitative treatment aimed at distinguishing between alternative classes of models and to provide information about which amino acid side chains are energetically important for binding. For brevity, we refer to association and disassociation rates in the following; these should be viewed as apparent or observed rates rather than rate constants as they are obtained directly from exponential fits of the data. The two disassociation rates, for example, correspond to the coefficients of the two exponentials obtained in the double exponential fits of the disassociation traces, while the three amplitudes discussed below are those associated with the two exponentials in the fit ("fast" and "slow") and with the very slow nonexponential phase.

The Multiple Dissociation Phases Do Not Result from Heterogeneity of SPR Attachment. Although kinetic heterogeneity in SPR experiments often results from heterogeneous attachment of the ligand to the BIAcore chip (*34*), this effect does not account for the observed fast, slow, and very slow phases. Dissociation phases with similar rates are observed in the reversed experiments (i.e., in κ binding to immobilized PLW) and in PLW binding to immobilized intact IgG. They are also observed when the V51C mutant is attached to the chip by a biotin-maleimide method (data not shown). The persistence of these kinetic phases despite different ligands and different coupling methods indicates that the kinetic heterogeneity is not caused by heterogeneity of the coupling of the ligand to the BIAcore chip, but by the presence of at least three kinetic species in the binding of PLW and κ in solution (*35*).

SPR Evidence for Binding at Both Sites. Comparison of sensorgrams for the binding of PLW and the mutants A20R, A20C, and V51C to κ indicate that both sites are capable of binding (Figure 6). The A20C and V51C dimers associate somewhat more slowly than PLW, but reach similar amplitudes and exhibit all three dissociation phases. By contrast, the A20R mutant exhibits a smaller amplitude for binding, and its dissociation is dominated by the fast phase; the slow and very slow phases are scarcely detectable. These observations demonstrate that both sites are capable of binding and have similar affinities. This conclusion is supported by SPR, radioimmunoassay and fluorescence binding studies of PLW and 75 point mutants, as described below. These studies demonstrate two binding-energy "hotspots" in the vicinity of site 1 and 2, with the largest contributions coming from Tyr34 (site 2) and Tyr36 (site 1).

Interpretation of Dissociation Phases. A key step in interpreting the BIAcore results is the identification of the fast and slow dissociation phases with molecular dissociation events. (The very slow phase is neglected in our analysis, since its nonexponential character suggests that it is not simple.) The simplest hypothesis is that the fast and slow dissociations correspond to dissociations from sites 1 and 2. If true, disruptive mutations in each binding site should predominantly affect the corresponding dissociation rate. Alternatively, the fast and slow dissociation phases could correspond to monovalent and bivalent binding of protein L with κ; in this case, the fast phase would be a composite of the dissociations from sites 1 and 2, and mutations in each site would affect both dissociation rates. To discern these

Table 1: Kinetics for the Interaction between Protein L and Ig κ Light Chains[a]

mutant	apparent association rate (10^6 M^{-1} s^{-1})	fast phase apparent dissociation rate (s^{-1})	slow phase apparent dissociation rate (s^{-1})	mutant	apparent association rate (10^6 M^{-1} s^{-1})	fast phase apparent dissociation rate (s^{-1})	slow phase apparent dissociation rate (s^{-1})
PLW	1.1 ± 0.13	0.087 ± 0.011	0.0063 ± 0.00046	E32G	1.0 ± 0.013	0.081 ± 0.0064	0.0065 ± 0.00106
E3A	0.75 ± 0.16	0.079 ± 0.0082	0.0063 ± 0.00057	E32I	0.78 ± 0.11	0.099 ± 0.022	0.0080 ± 0.00193
V4A	0.84 ± 0.16	0.10 ± 0.012	0.0073 ± 0.0012	A33G	0.94 ± 0.032	0.13 ± 0.011	0.0088 ± 0.00053
T5A	0.94 ± 0.13	0.092 ± 0.0022	0.0069 ± 0.00041	A33V	0.59 ± 0.016	0.079 ± 0.0009	0.0082 ± 0.00003
I6A	0.67 ± 0.11	0.097 ± 0.0088	0.0071 ± 0.00069	Y34A	0.58 ± 0.049	0.13 ± 0.013	0.0098 ± 0.0015
I6V	0.81 ± 0.087	0.098 ± 0.0094	0.0069 ± 0.00016	Y34H	0.66 ± 0.006	0.091 ± 0.0068	0.0082 ± 0.00004
K7A	0.66 ± 0.17	0.099 ± 0.011	0.0064 ± 0.00015	A35G	1.0 ± 0.036	0.10 ± 0.016	0.0083 ± 0.0013
A8G	0.98 ± 0.004	0.080 ± 0.0037	0.0062 ± 0.00020	Y36A	0.18 ± 0.070	0.12 ± 0.0025	0.020 ± 0.00177
N9A	0.79 ± 0.054	0.11 ± 0.0062	0.0077 ± 0.00048	Y36F	0.66 ± 0.16	0.096 ± 0.0095	0.0074 ± 0.00122
L10A	0.86 ± 0.11	0.096 ± 0.0067	0.0097 ± 0.00096	A37G	0.90 ± 0.002	0.078 ± 0.0020	0.0060 ± 0.00037
I11A	1.2 ± 0.021	0.090 ± 0.013	0.0066 ± 0.0012	D38A	1.1 ± 0.016	0.077 ± 0.0038	0.0066 ± 0.00011
F12A	0.87 ± 0.017	0.080 ± 0.0042	0.0069 ± 0.00056	D38G	0.93 ± 0.077	0.11 ± 0.0054	0.0086 ± 0.00107
F12L	1.0 ± 0.079	0.086 ± 0.010	0.0069 ± 0.00075	T39G	1.1 ± 0.036	0.081 ± 0.0054	0.0065 ± 0.00033
A13P	0.87 ± 0.021	0.082 ± 0.0069	0.0076 ± 0.00052	L40A	0.94 ± 0.026	0.080 ± 0.0014	0.0081 ± 0.00040
N14A	0.67 ± 0.095	0.083 ± 0.0004	0.0065 ± 0.00029	K41A	0.71 ± 0.012	0.066 ± 0.0020	0.0059 ± 0.00032
G15A	0.58 ± 0.021	0.081 ± 0.014	0.0071 ± 0.00080	K42A	0.71 ± 0.032	0.078 ± 0.0038	0.0056 ± 0.00003
S16A	1.2 ± 0.25	0.088 ± 0.013	0.0068 ± 0.00069	N44A	0.71 ± 0.018	0.075 ± 0.0071	0.0059 ± 0.00067
T17A	0.90 ± 0.040	0.089 ± 0.011	0.0068 ± 0.0013	G45A	1.1 ± 0.012	0.072 ± 0.0003	0.0066 ± 0.00001
Q18A	0.48 ± 0.001	0.10 ± 0.013	0.010 ± 0.0012	E46A	1.0 ± 0.024	0.10 ± 0.0006	0.0078 ± 0.00002
T19A	1.1 ± 0.10	0.090 ± 0.0044	0.0070 ± 0.00029	W47Y	3.2 ± 0.24	0.10 ± 0.0039	0.0077 ± 0.00071
A20V	1.1 ± 0.19	0.098 ± 0.011	0.0096 ± 0.00019	T48A	0.79 ± 0.018	0.081 ± 0.0005	0.0067 ± 0.00007
A20G	0.89 ± 0.11	0.088 ± 0.0050	0.0071 ± 0.00051	V49A	0.94 ± 0.024	0.085 ± 0.0075	0.0065 ± 0.00023
A20R	0.13 ± 0.017	0.11 ± 0.021	0.026 ± 0.0036	D50A	0.89 ± 0.033	0.080 ± 0.0060	0.0062 ± 0.00075
A20C	0.22 ± 0.060	0.075 ± 0.020	0.0051 ± 0.0014	V51A	0.59 ± 0.002	0.12 ± 0.013	0.0091 ± 0.00035
E21A	1.0 ± 0.037	0.079 ± 0.0080	0.0070 ± 0.0012	V51C	0.19 ± 0.087	0.047 ± 0.0046	0.0055 ± 0.0014
F22A	0.54 ± 0.080	0.11 ± 0.023	0.0094 ± 0.00070	A52G	0.88 ± 0.022	0.089 ± 0.0032	0.0074 ± 0.00053
F22L	0.81 ± 0.11	0.097 ± 0.0086	0.0070 ± 0.00057	D53A	0.76 ± 0.008	0.090 ± 0.0002	0.0057 ± 0.00002
F22W	0.37 ± 0.082	0.097 ± 0.025	0.0055 ± 0.00023	K54A	0.86 ± 0.037	0.091 ± 0.0018	0.0073 ± 0.00031
K23A	1.1 ± 0.012	0.091 ± 0.0072	0.0073 ± 0.0012	G55A	0.14 ± 0.041	0.053 ± 0.0099	0.0057 ± 0.00009
G24A	1.4 ± 0.45	0.10 ± 0.0044	0.0075 ± 0.00074	Y56A	0.88 ± 0.014	0.075 ± 0.013	0.0069 ± 0.00068
T25A	0.75 ± 0.001	0.079 ± 0.0033	0.0068 ± 0.00032	Y56L	0.60 ± 0.017	0.074 ± 0.0085	0.0068 ± 0.00001
F26G	0.72 ± 0.047	0.13 ± 0.0002	0.0099 ± 0.00045	T57A	1.3 ± 0.028	0.12 ± 0.0033	0.0090 ± 0.00009
F26L	0.79 ± 0.087	0.12 ± 0.014	0.0094 ± 0.00095	L58A	0.58 ± 0.028	0.092 ± 0.0088	0.0075 ± 0.00118
E27A	0.43 ± 0.054	0.085 ± 0.0026	0.0072 ± 0.00015	N59A	0.81 ± 0.083	0.098 ± 0.0022	0.0077 ± 0.00020
K28G	0.90 ± 0.20	0.097 ± 0.0098	0.0074 ± 0.00085	I60A	0.71 ± 0.012	0.081 ± 0.0051	0.0074 ± 0.00095
A29G	0.73 ± 0.13	0.087 ± 0.011	0.0070 ± 0.00047	I60V	1.2 ± 0.020	0.095 ± 0.0048	0.0082 ± 0.00070
T30A	0.61 ± 0.065	0.034 ± 0.0012	0.0072 ± 0.00077	K61A	0.95 ± 0.014	0.095 ± 0.0027	0.0076 ± 0.00099
S31A	1.0 ± 0.17	0.11 ± 0.016	0.0082 ± 0.00111	F62V	0.80 ± 0.10	0.11 ± 0.011	0.0082 ± 0.00011
S31G	0.71 ± 0.027	0.083 ± 0.012	0.0074 ± 0.00063	F62L	1.0 ± 0.098	0.089 ± 0.0086	0.0064 ± 0.00055

[a] Apparent association and dissociation rates as measured by SPR. Values given are mean ± SD ($n = 2-9$).

possibilities, we carried out SPR experiments on all 75 of our point mutants. The fast and slow phases are correlated in most mutants (Figure 7a); linear regression leads to the equation $\Delta\Delta G^{\ddagger}_{off,slow} = 0.85\Delta\Delta G^{\ddagger}_{off,fast}$, where $\Delta G^{\ddagger}_{off}$ represents the activation free energy for dissociation. It is unlikely that this correlation is due to fitting artifacts, given the roughly 10-fold difference in the fast and slow rates (Table 1). The changes $\Delta\Delta G^{\ddagger}_{off}$ are not correlated with the conformational destabilization $\Delta\Delta G^{\ddagger}_{fold}$ caused by these mutations (*24*), and furthermore, the structures of several protein L variants have also been determined by X-ray crystallography and no large differences have been seen between the different variants (*10*, *18*−*20*). Hence, the observation that mutations in *both* binding sites affect *both* dissociation rates suggests that the second hypothesis is correct, i.e., that the fast and slow phases correspond to monovalent and bivalent binding of PLW to κ and that the fast phase is composite.

Four outliers of the overall correlation in the fast and slow dissociation rate are worth noting (Figure 7a). The A20R mutant (which appears to have abolished site 1 binding while preserving site 2 binding) and another site 1 mutant Y36A exhibit slightly elevated rates for the fast phase (0.107 and 0.119 s^{-1}, respectively) but exceptionally high rates for the slow phase (0.026 and 0.020 s^{-1}, respectively). We interpret this observation as indicating that bivalent binding has been weakened drastically in these two mutants. Similarly, the site 2 mutants T30A and G55A have normal rates for the slow phase (0.007 and 0.006 s^{-1}, respectively) but unusually low rates for the fast phase (0.034 and 0.053 s^{-1}, respectively).

Effects of Mutations on Association as Measured by SPR. In contrast to the dissociation, the association of PLW to immobilized κ is dominated by a single-exponential phase (Figure 5a). For PLW, the rate of this single association phase is 1.1×10^6 M^{-1} s^{-1} under our conditions (Table 1). In general, the association rates for the 75 mutants are similar, with a mean and standard deviation of $0.82 \pm 0.24 \times 10^6$ M^{-1} s^{-1} (Table 1). However, the A20R, Y36A, and G55A mutants all have significantly lower association rates (0.13, 0.18, and 0.14×10^6 M^{-1} s^{-1}, respectively; Table 1, Figure 7b,c), consistent with our above interpretation that these mutations disrupt binding at either site 1 (A20R and Y36A) or site 2 (G55A). The adjacent site 1 mutants Q18A and F22W and the site 2 mutant E27A also lower the association

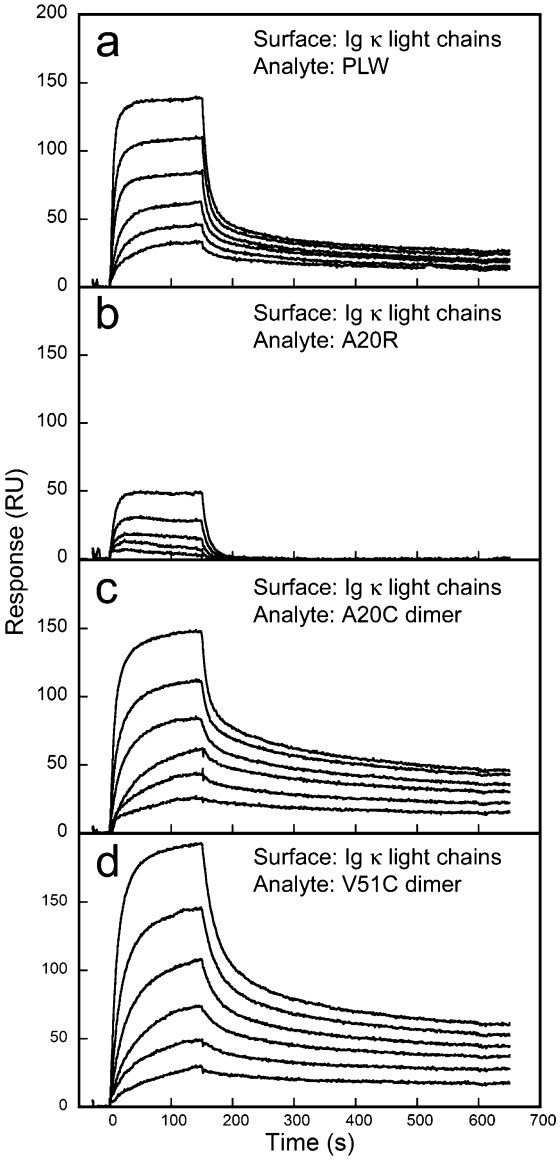

FIGURE 6: (a−d) BIAcore sensorgrams for PLW and its mutants A20R, A20C, and V51C. The data indicate that the mutants binds to Ig κ light chain, despite the disruptions of sites 1 and 2. The affinities of the two sites appear comparable, although site 1 may have slightly higher affinity than site 2, judging from the sensorgrams for V51C and A20C, respectively.

rate significantly (0.48, 0.34, and 0.43 $\times$ 10^6 M^{-1} s^{-1}, respectively) but not by more than two standard deviations (Table 1, Figure 7b,c). Similarly, the site 1 mutant G24A and the site 2 (revertant) mutant W47Y *increase* the association rate by more than two standard deviations (Table 1, Figure 7b,c).

SPR Kinetic Titrations. To estimate the dissociation constants for the monovalent and bivalent binding modes, we plotted the maximal amplitudes of the fast, slow, and very slow dissociation phases (measured after 10 min of association) as a function of the protein L concentration in solution during the association period. The three phases form three distinct titration curves of roughly 900, 17, and 5 nM equilibrium dissociation constants (K_D), respectively (Figure 8a,b). The midpoints of these transitions are reproducible for different BIAcore chips and do not depend on the preparation of the chip. However, the relative amplitudes of the titration curves at saturating PLW concentrations vary

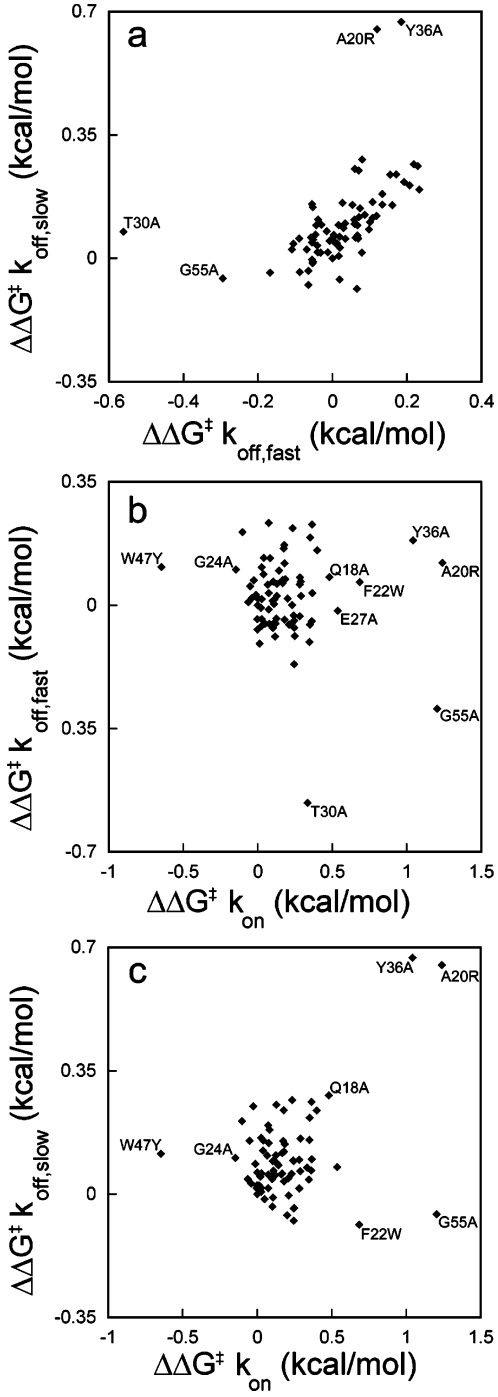

FIGURE 7: Effects of mutations on the two apparent dissociation rates $k_{off,slow}$ and $k_{off,fast}$ and the apparent association rate k_{on} for PLW binding to Ig κ light chain. (a) Plot of $\Delta\Delta G^{\ddagger}_{off,slow}$ versus $\Delta\Delta G^{\ddagger}_{off,fast}$. Mutations cause *correlated* changes in the two dissociation rate constants $k_{off,slow}$ and $k_{off,fast}$. Four outlier mutations can be noted; the A20R and Y36A mutants have exceptionally high $k_{off,slow}$ values but normal $k_{off,fast}$ values, whereas the T30A and G55A mutants have exceptionally low $k_{off,fast}$ values but normal $k_{off,slow}$ values. (b,c) Plots of $\Delta\Delta G^{\ddagger}_{off,fast}$ versus $\Delta\Delta G^{\ddagger}_{on}$ and $\Delta\Delta G^{\ddagger}_{off,slow}$ versus $\Delta\Delta G^{\ddagger}_{on}$ respectively. Mutations cause *uncorrelated* changes in k_{on} and the two apparent dissociation rates. Three of the four dissociation-rate outlier mutants (A20R, Y36A, and G55A) are also outliers in the association rate; only the T30A mutant has a normal association rate. Other mutations in site 1 (Q18A, F22W, G24A) and in site 2 (E27A, W47Y) cause significant changes in the association rate as well. The $\Delta\Delta G^{\ddagger}$ values were calculated using the apparent rates.

Table 2: Equilibrium Dissociation Constants Estimated from SPR Titrations[a]

	K_D (fast) nM	$\Delta\Delta G$ (fast) kcal/mol	K_D (slow) nM	$\Delta\Delta G$ (slow) kcal/mol	K_D (v·slow) nM	$\Delta\Delta G$ (v·slow) kcal/mol
PLW	900	0.0	17	0.0	4.9	0.0
Q18A	720	−0.13	21	+0.13	88	**+1.71**
A20R	630	−0.21	335	**+1.78**	551	**+2.80**
F22A	2300	+0.55	66	+0.82	472	**+2.71**
F26L	2200	+0.53	30	+0.35	92	**+1.73**
E27A	780	−0.08	10	−0.28	7.5	+0.25
T30A	450	−0.41	27	+0.28	3.4	−0.22
Y34A	1800	+0.41	192	**+1.45**	371	**+2.56**
Y36A	940	+0.03	170	**+1.37**	488	**+2.73**
V51A	1200	+0.17	28	+0.30	38	**+1.21**

[a] Values are mean values from at least two experiments. Bold-face type indicates changes in binding free energy over 1.0 kcal/mol.

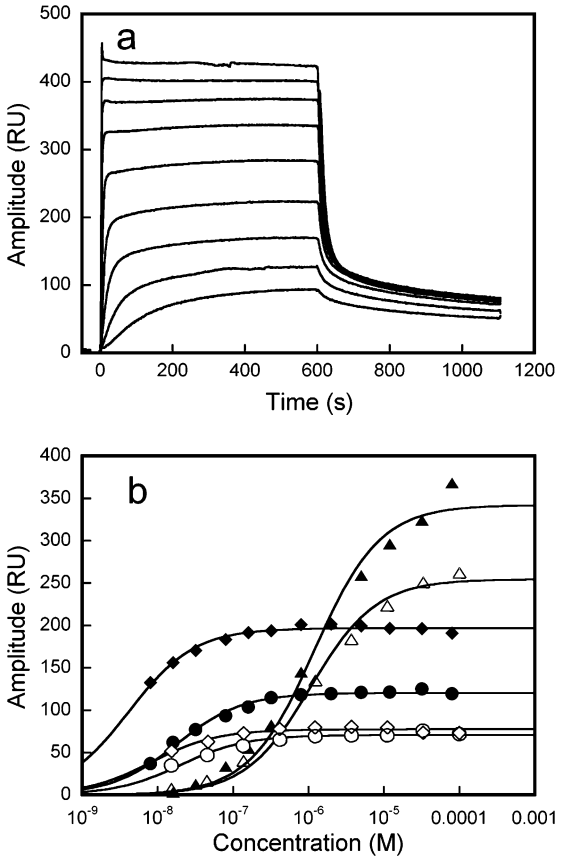

FIGURE 8: SPR kinetic titration curves. (a) Typical sensorgrams for the SPR kinetic titration experiments. The association phase is allowed to come to equilibrium for different concentrations of PLW (15 nM to 100 μM) in the running buffer; the amplitudes of the subsequent fast, slow, and very slow dissociation phases are then plotted versus PLW concentration in panel b. (b) Two titrations for PLW carried out on different BIAcore chips. The fast (triangles), slow (circles), and very slow (diamonds) phases from two experiments are shown with open and closed symbols. The open symbols correspond to the experiment shown in panel a. PLW appear to titrate with equilibrium dissociation constants of roughly 900, 17, and 5 nM for the fast, slow, and very slow phases, respectively (Table 2). The *midpoints* of the transitions do not vary with the BIAcore chip, but the *amplitudes* depend on the density of Ig κ light chains on the chip.

significantly between different chips; a chip decorated with a lower density of κ has higher saturation amplitude of the fast phase relative to those of the slow and very slow phases, when compared to a chip decorated with a greater density of κ. This is consistent with the hypothesis that the slow phases result from the binding of multiple κ to a single PLW molecule since a higher density of κ on the surface gives more sites where PLW can bind to multiple κ.

Kinetic titration experiments were also carried out for the site 1 mutants Q18A, A20R, F22A, and Y36A as well as for the site 2 mutants F26L, E27A, T30A, Y34A, and V51A. The total saturation amplitudes of these mutant titrations were similar to the PLW titration carried out on the same BIAcore chip. The effects of the mutations can therefore be characterized by the shift in the equilibrium dissociation constants of the three phases (Table 2). The fast-phase titration is relatively insensitive to mutation; the largest effects (roughly 2-fold changes in K_D) are observed for the site 1 mutation F22A and the site 2 mutations F26L, T30A, and Y34A. The slow phase is much more sensitive to mutations, with 4−20-fold increases in K_D for the site 1 mutants A20R, F22A, and Y36A and a 10-fold increase in K_D for the site 2 mutant Y34A. The very slow phase is even more sensitive to mutation, with 20−140-fold increases in K_D for the site 1 mutants Q18A, A20R, F22A, and Y36A and 25−120- fold increases in K_D for the site 2 mutants F26L, Y34A, and V51A. The site 2 mutations E27A and T30A had little effect on any of the titrations. The change in binding free energy $\Delta\Delta G$ of the fast phase is not correlated with those of the slow and very slow phases; by contrast, the change in binding free energy $\Delta\Delta G$ of the slow phase is significantly correlated with that of the very slow phase. These observations are likewise consistent with the hypothesis that the slow phases result from the binding of multiple κ to a single PLW molecule, whereas the fast phase is a composite of site 1 and site 2 binding.

The SPR Titration Data Eliminate the Sequential Model of PLW−V_κ Binding. A sequential model V_κ + PLW ⇔ C1 ⇔ C2 has been used to describe the kinetics of PLW−V_κ binding (*21*, *23*); here, C1 and C2 represent two forms of the PLW−V_κ complex. This model is a special case of the general three-species model

$$V_\kappa + \mathrm{PLW} \Leftrightarrow \mathrm{C1}$$

$$V_\kappa + \mathrm{PLW} \Leftrightarrow \mathrm{C2}$$

$$\mathrm{C1} \Leftrightarrow \mathrm{C2}$$

This general model can also represent the binding of PLW at two sites (e.g., with each edge of its β-sheet) to a single binding site on V_κ, with the optional complication that the two types of complexes may interconvert without the dissociation of PLW. Although such models do produce multiple exponential phases (*35*), *no such three-species model can account for the kinetic heterogeneity observed in our experiments (i.e., the fast, slow, and very slow dissociation phases)*. The reason for this failure is that all such models predict that the ratio of the equilibrium amplitudes of the various dissociations is independent of the concentration of PLW in the flowing solution during the association phase. This is contradicted by the observation that these equilibrium amplitudes follow independent titration curves (Figure 8b). Moreover, since the dissociation constants K_D of the titration curves differ roughly 50-fold (Figure 8b), the putative weak-binding site on PLW should be populated much less than the strong-binding site if they competed for a single binding

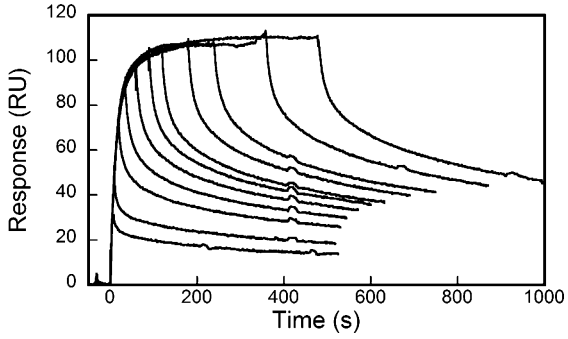

FIGURE 9: Sensorgram for a typical time-lapse experiment for PLW binding to Ig κ light chains. 75 nM PLW was flowed over the Ig κ light chain surface and the association was interrupted at various times (6−480 s).

site on V_k. This is contrary to the SPR titration data showing that the saturation amplitude of the fast dissociation phase is much *larger* than those of the slow and very slow dissociation phases (Figure 8b). Therefore, neither the sequential model nor the two-independent-binding-sites model can account for the three dissociation phases. This is consistent with our arguments that the phases differ in being monovalent or multivalent.

SPR Time Laps Experiments. To investigate the rate at which the fast disassociating species is converted to the two slowly disassociating species, we carried out time-lapse experiments using SPR (Figure 9). As expected, the amplitudes of all three dissociation phases increase with the association time. However, for association times above 200 s, the fast-phase amplitude decreases with increasing association time, with a corresponding increase in the very slow phase amplitude (Supporting Information, Figure 1). This effect is observed at all concentrations of PLW in the flowing solution, in both PLW and all mutants tested. If this change in the relative amplitudes of the fast and slow/very slow phases were due to a conformational change, the ratio of the amplitudes at a given time point should be independent of protein concentration (the conversion in this case is a first-order process). However, the ratio of the amplitudes is observed to be concentration dependent. The simplest interpretation is that monomeric complexes are being converted to higher-order complexes on the chip, and that the fast phase corresponds to monovalently bound complexes, while the slow phases correspond to multivalently bound complexes.

Fluorescence and Radioimmunoassay Experiments. The binding titrations of PLW and κ were also monitored by fluorescence and radioimmunoassays. The radioimmunoassays show that fully half of the saturation amount of PLW is bound already at 2 nM of free PLW (Figure 10a). The ability of several mutants to inhibit the binding of PLW to immobilized κ or intact IgG was also tested by radioimmunoassay (Figure 10a,b). By this criterion, the site 2 T30A mutation appears to strengthen the binding, whereas the mutations F26L, Q18A, F22A, Y34A, and Y36A appear to weaken the binding in increasing order. This order agrees with the $\Delta\Delta G$ values obtained from the SPR kinetic titrations (Table 2), except that the F26L mutation weakens the binding more than the Q18A mutation, judging from the $\Delta\Delta G$ values. Similarly, some mutants were tested for their ability to inhibit

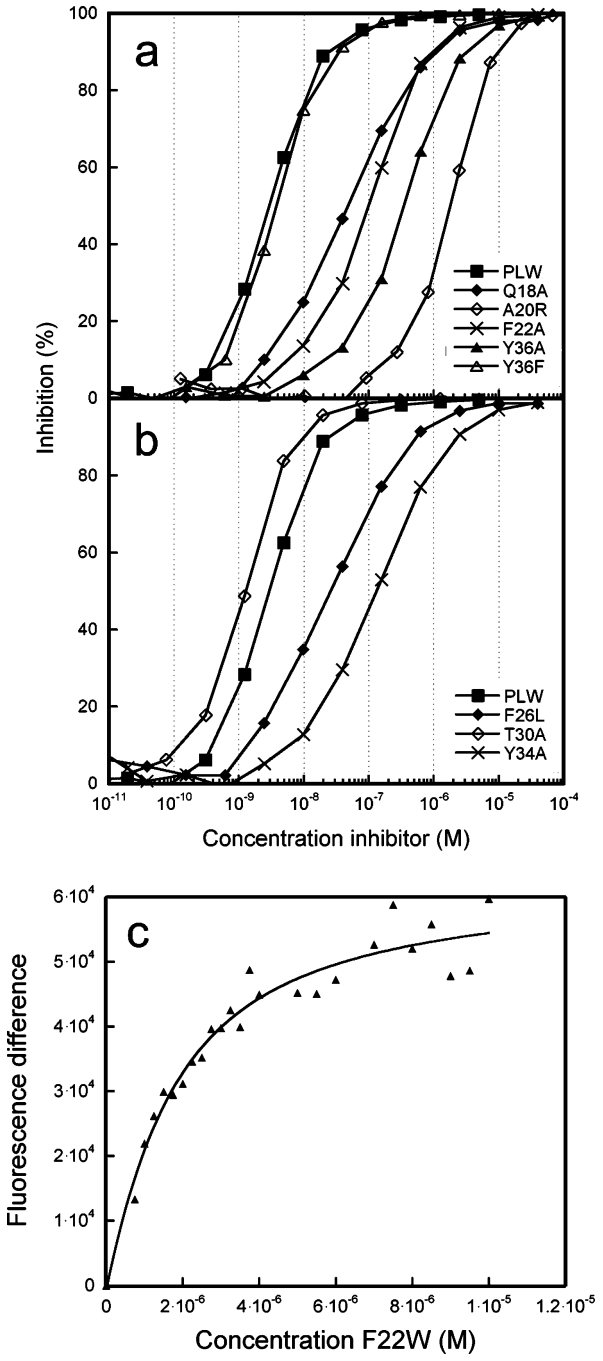

FIGURE 10: (a) Unlabeled PLW and various site 1 PLW mutants were used to inhibit the binding of I^{125}-PLW to Ig κ light chains immobilized in a microtiter plate. (b) Unlabeled PLW and various site 2 PLW mutants were used to inhibit the binding of I^{125}-PLW to Ig κ light chains immobilized in microtiter plates. (c) Fluorescence binding assay for the F22W mutant and Ig κ light chain.

binding to polyclonal IgG (data not shown). The IgG data agreed with the SPR and radioimmunoassay experiments carried out on κ.

The fluorescence titration of the F22W mutant shows a single titration of K_D of 218 nM (Figure 10c), which is consistent with the equilibrium dissociation constants measured by fluorescence in earlier studies (*21*, *23*) and with those estimated in the BIAcore titrations for monovalent binding (Table 2), respectively. This supports our model that wild-type protein L binds bivalently (with a low nM dissociation constant), whereas mutants in which site 1 or

Table 3: Computational Alanine Scanning[a]

mutation	$\Delta\Delta G$ (kcal mol^{-1})
E3A	−0.29
V4A	0.00
T5A	0.01
I6A	0.01
K7A	0.10
V8A*(A)	0.00
N9A	−0.16
L10A	0.13
I11A	0.00
F12A	−0.04
D14A*(N)	−0.01
K16A*(S)	0.39
I17A*(T)	−0.01
Q18A	**1.84**
T19A	0.00
E21A	0.37
F22A	**1.38**
K23A	0.26
T25A	0.00
F26A	**2.18**
E27A	**1.48**
E28A*(K)	0.00
T30A	0.28
A31A*(S)	
E32A	0.40
Y34A	**2.41**
R35A*(A)	1.12
Y36A	**2.72**
D38A	**1.72**
L39A*(T)	0.56
L40A	0.22
A41A*(K)	
K42A	0.00
V43A	0.15
N44A	0.01
E46A	−0.01
Y47A*(W)	0.97
T48A	0.24
A49A*(V)	0.00
D50A	0.10
L51A*(V)	**1.64**
E52A*(A)	0.07
D53A	0.00
N56A*(Y)	0.05
H57A*(T)	−0.01
M58A*(L)	0.05
N59A	0.00
I60A	0.05
K61A	−0.02

[a] Predicted binding-energy hotspots are indicated in bold-face type. Sequence differences between the B1 domain of our protein L construct and that found in the crystal structure (*18*) are indicated by an asterisk, where the residue of our protein L construct is given in parentheses.

site 2 binding is disrupted bind monovalently with high nanomolar affinities.

Agreement with Computational Alanine-Scanning Mutagenesis. As described above, several experimental probes implicate the same amino acid side chains (Q18, F22, F26, Y34, Y36, V51) as contributing most strongly to the binding of PLW and κ. These results are consistent with computational estimates of the $\Delta\Delta G$ for these mutants (see Methods). Computational alanine scanning of all nonalanyl, nonglycyl residues in PLW identifies the side chains of Q18, F22, F26, E27, Y34, Y36, D38, and V51 as binding-energy hotspots, whereas mutations outside of the binding sites identified crystallographically do not affect binding (Table 3). With the exception of the E27A and D38A mutants, these computational predictions agree with the experimental data for $\Delta\Delta G$ (Tables 1 and 2). Taken together, our experimental and computational results provide strong evidence that PLW binds κ primarily at the two crystallographic sites.

Table 4: Relative Contributions of Side Chain−Side Chain (sc-sc), Side Chain−Main Chain (sc-mc) and Main Chain−Main Chain (mc-mc) Hydrogen Bonds to the Total Number of Hydrogen Bonds Found in the Interface

	PpL − Ig κ light chain interface[a]		
	site 1	site 2	generic interface average[b]
sc-sc	0.17	0.12	0.36
sc-mc	0.33	0.50	0.40
mc-mc	0.50	0.38	0.24

[a] As identified by Graille et al., 2001 (*18*). [b] Taken from Lo Conte et al., 1999 (*44*).

CONCLUSIONS

Our experimental and computational studies indicate that PLW binds with significant affinity to κ at *both* of its binding sites identified in the crystal structure (*18*). The ability of PLW to bind with both edges of its β-sheet is also observed in its own crystal structure (*10*) and in structures of the corresponding domain in protein G (*36*−*40*). Such ambidextrous binding of PLW renders it relatively robust against mutations (Tables 1 and 2), since the elimination of one binding site by a sufficiently destabilizing mutation leaves another binding site intact. In contrast to previous suggestions (*41*), our data suggest that the affinity of site 2 for κ is only slightly less than that of site 1 (*22*).

The primary "hot spots" for PLW-κ binding are the two tyrosines Tyr34 and Tyr36, which belong to sites 2 and 1, respectively (Figure 1a,b). Tyrosines have been implicated in "hot spots" of other protein−protein complexes (*42*), e.g., Tyr434 and Tyr437 of ribonuclease inhibitor complexed with ribonuclease (*43*). It is also interesting to note that the key β-strand in V_κ that binds to both sites in PLW is very rich in serines (Ser7, Ser9, Ser10, Ser12, Ser14), which form numerous intermolecular hydrogen bonds (*18*). In particular, Ser9 is replaced by leucine in $V_{\kappa II}$, which may partly account for the lack of affinity between PLW and $V_{\kappa II}$ domains.

In general, the effects of PLW mutations on PLW-κ binding are smaller than those observed in other protein−protein complexes studied by alanine-scanning mutagenesis (*42*). Moreover, comparatively few residues of PLW affect the binding significantly when they are replaced by alanines. This is consistent with the unusually high percentage of main chain interactions in the PLW−κ interfaces (Table 4), which may account in part for the ability of protein L to bind to V_κ from many different species (*15*). The functional requirement of binding diverse κ sequences favor backbone hydrogen bonding, rather than specific side chain interactions, in the binding site. Ambidextrous binding of the B1−B5 domains yields 10 binding sites in naturally occurring protein L, thus ensuring avid binding despite the lack of numerous, strong side chain−side chain interactions.

ACKNOWLEDGMENT

We thank Drs. Branislava Savic and Qian Yi for valuable help.

SUPPORTING INFORMATION AVAILABLE

Plots of a time lapse experiment of PLW association with κ light chains (Figure 1). This material is available free of charge via the Internet at http://pubs.acs.org.

REFERENCES

1. Björck, L. (1988) Protein L. A novel bacterial cell wall protein with affinity for Ig L chains. *J. Immunol. 140*, 1194−7.
2. Kastern, W., Holst, E., Nielsen, E., Sjöbring, U., and Björck, L. (1990) Protein L, a bacterial immunoglobulin-binding protein and possible virulence determinant. *Infect. Immun. 58*, 1217−22.
3. Ricci, S., Medaglini, D., Marcotte, H., Olsen, A., Pozzi, G., and Björck, L. (2001) Immunoglobulin-binding domains of peptostreptococcal protein L enhance vaginal colonization of mice by *Streptococcus gordonii*. *Microb. Pathog. 30*, 229−35.
4. Patella, V., Casolaro, V., Björck, L., and Marone, G. (1990) Protein L. A bacterial Ig-binding protein that activates human basophils and mast cells. *J. Immunol. 145*, 3054−61.
5. Genovese, A., Bouvet, J. P., Florio, G., Lamparter-Schummert, B., Björck, L., and Marone, G. (2000) Bacterial immunoglobulin superantigen proteins A and L activate human heart mast cells by interacting with immunoglobulin E. *Infect. Immun. 68*, 5517−24.
6. Kastern, W., Sjöbring, U., and Björck, L. (1992) Structure of peptostreptococcal protein L and identification of a repeated immunoglobulin light chain-binding domain. *J. Biol. Chem. 267*, 12820−5.
7. Wikström, M., Sjöbring, U., Kastern, W., Björck, L., Drakenberg, T., and Forsén, S. (1993) Proton nuclear magnetic resonance sequential assignments and secondary structure of an immunoglobulin light chain-binding domain of protein L. *Biochemistry 32*, 3381−3386.
8. Gu, H., Yi, Q., Bray, S. T., Riddle, D. S., Shiau, A. K., and Baker, D. (1995) A phage display system for studying the sequence determinants of protein folding. *Protein Sci. 4*, 1108−17.
9. Wikström, M., Drakenberg, T., Forsén, S., Sjöbring, U., and Björck, L. (1994) Three-dimensional solution of an immunoglobulin light chain-binding domain of protein L. Comparison with the IgG-binding domain of protein G. *Biochemistry 33*, 14011−7.
10. O'Neill, J. W., Kim, D. E., Baker, D., and Zhang, K. Y. (2001) Structures of the B1 domain of protein L from *Peptostreptococcus magnus* with a tyrosine to tryptophan substitution. *Acta Crystallogr., Sect. D: Biol. Crystallogr. 57*, 480−7.
11. Björck, L., and Kronvall, G. (1984) Purification and some properties of streptococcal protein G, a novel IgG-binding reagent. *J. Immunol. 133*, 969−74.
12. Reis, K., Ayoub, E., and Boyle, M. (1984) Streptococcal Fc receptors. I. Isolation and partial characterization of the receptor from a group C streptococcus. *J. Immunol. 132*, 3091−7.
13. Gronenborn, A. M., Filpula, D. R., Essig, N. Z., Achari, A., Whitlow, P. T., Wingfield, P. T., and Clore, G. M. (1991) A Novel Highly Stable Fold of the Immunoglobulin Binding Domain of Streptococcal Protein G. *Science 253*, 657−61.
14. Forsgren, A., and Sjöquist, J. (1966) "Protein A" from *S. aureus*. I. Pseudo-immune reaction with human gamma-globulin. *J. Immunol. 97*, 822−7.
15. Åkerström, B., and Björck, L. (1989) Protein L: an immunoglobulin light chain-binding bacterial protein. Characterization of binding and physicochemical properties. *J. Biol. Chem. 264*, 19740−6.
16. de Château, M., Nilson, B. H. K., Erntell, M., Myhre, E., Magnusson, C. G. M., Åkerström, B., and Björck, L. (1993) On the interaction between protein L and immunoglobulins of various mammalian species. *Scand. J. Immunol. 37*, 399−405.
17. Nilson, B. H. K., Solomon, A., Björck, L., and Åkerström, B. (1992) Protein L from *Peptostreptococcus magnus* binds the κ light chain variable domain. *J. Biol. Chem. 267*, 2234−9.
18. Graille, M., Stura, E. A., Housden, N. G., Beckingham, J. A., Bottomley, S. P., Beale, D., Taussig, M. J., Sutton, B. J., Gore, M. G., and Charbonnier, J. B. (2001) Complex between *Peptostreptococcus magnus* Protein L and a Human Antibody Reveals Structural Convergence in the Interaction Modes of Fab Binding Proteins. *Structure 9*, 679−87.
19. Graille, M., Harrison, S., Crump, M. P., Findlow, S. C., Housden, N. G., Muller, B. H., Battail-Poirot, N., Sibai, G., Sutton, B. J., Taussig, M. J., Jolivet-Reynaud, C., Gore, M. G., and Stura, E. A. (2002) Evidence for plasticity and structural mimicry at the immunoglobulin light chain-protein L interface. *J. Biol. Chem. 277*, 47500−6.
20. Stura, E. A., Graille, M., Housden, N. G., and Gore, M. G. (2002) Protein L mutants for the crystallization of antibody fragments. *Acta Crystallogr. D Biol. Crystallogr. 58*, 1744−8.
21. Beckingham, J. A., Bottomley, S. P., Hinton, R., Sutton, B. J., and Gore, M. G. (1999) Interactions between a single immunoglobulin-binding domain of protein L from *Peptostreptococcus magnus* and a human κ light chain. *Biochem. J. 340*, 193−9.
22. Wikström, M., Sjöbring, U., Drakenberg, T., Forsen, S., and Björck, L. (1995) Mapping of the immunoglobulin light chain-binding site of protein L, *J. Mol. Biol. 250*, 128−33.
23. Beckingham, J. A., Housden, N. G., Muir, N. M., Bottomley, S. P., and Gore, M. G. (2001) Studies on a single immunoglobulin-binding domain of protein L from *Peptostreptococcus magnus*: the role of tyrosine-53 in the reaction with human IgG. *Biochem. J. 353*, 395−401.
24. Kim, D. E., Fisher, C., and Baker, D. (2000) A breakdown of symmetry in the folding transition state of protein L. *J. Mol. Biol. 298*, 971−84.
25. Scalley, M. L., Yi, Q., Gu, H., McCormack, A., Yates, J. R. r., and Baker, D. (1997) Kinetics of folding of the IgG binding domain of peptostreptococcal protein L. *Biochemistry 36*, 3373−82.
26. Myszka, D. G. (1999) Improving biosensor analysis. *J. Mol. Recognit. 12*, 279−84.
27. Kortemme, T., and Baker, D. (2002) A simple physical model for binding energy hot spots in protein−protein complexes. *Proc. Natl. Acad. Sci. U.S.A. 99*, 14116−21.
28. Kuhlman, B., and Baker, D. (2000) Native protein sequences are close to optimal for their structures. *Proc. Natl. Acad. Sci. U.S.A. 97*, 10383−8.
29. Chevalier, B. S., Kortemme, T., Chadsey, M. S., Baker, D., Monnat, R. J., and Stoddard, B. L. (2002) Design, activity, and structure of a highly specific artificial endonuclease. *Mol. Cell 10*, 895−905.
30. Epp, O., Colman, P., Fehlhammer, H., Bode, W., Schiffer, M., Huber, R., and Palm, W. (1974) Crystal and molecular structure of a dimer composed of the variable portions of the Bence-Jones protein REI. *Eur. J. Biochem. 45*, 513−24.
31. Huang, D. B., Chang, C. H., Ainsworth, C., Brunger, A. T., Eulitz, M., Solomon, A., Stevens, F. J., and Schiffer, M. (1994) Comparison of crystal structures of two homologous proteins: structural origin of altered domain interactions in immunoglobulin light-chain dimers. *Biochemistry 33*, 14848−57.
32. Roussel, A., Spinelli, S., Deret, S., Navaza, J., Aucouturier, P., and Cambillau, C. (1999) The structure of an entire noncovalent immunoglobulin kappa light-chain dimer (Bence-Jones protein) reveals a weak and unusual constant domains association. *Eur. J. Biochem. 260*, 192−9.
33. Stevens, F. J., Westholm, F. A., Solomon, A., and Schiffer, M. (1980) Self-association of human immunoglobulin kappa I light chains: role of the third hypervariable region. *Proc. Natl. Acad. Sci. U.S.A. 77*, 1144−8.
34. Rich, R. L., and Myszka, D. G. (2001) Survey of the year 2000 commercial optical biosensor literature. *J. Mol. Recognit. 14*, 273−94.
35. Sendak, R. A., Rothwarf, D. M., Wedemeyer, W. J., Houry, W. A., and Scheraga, H. A. (1996) Kinetic and thermodynamic studies of the folding/unfolding of a tryptophan-containing mutant of ribonuclease A. *Biochemistry 35*, 12978−92.
36. Achari, A., Hale, S. P., Howard, A. J., Clore, G. M., Gronenborn, A. M., Hardman, K. D., and Whitlow, M. (1992) 1.67-Å X-ray structure of the B2 immunoglobulin-binding domain of streptococcal protein G and comparison to the NMR structure of the B1 domain. *Biochemistry 31*, 10449−57.
37. Gallagher, T., Alexander, P., Bryan, P., and Gilliland, G. L. (1994) Two crystal structures of the B1 immunoglobulin-binding domain of streptococcal protein G and comparison with NMR. *Biochemistry 33*, 4721−9.

38. Enokizono, J., Wikström, M., Sjöbring, U., Björck, L., Forsén, S., Arata, Y., Kato, K., and Shimada, I. (1997) NMR analysis of the interaction between protein L and Ig light chains. *J. Mol. Biol. 270*, 8−13.
39. Derrick, J. P., and Wigley, D. B. (1992) Crystal structure of a streptococcal protein G domain bound to an Fab fragment. *Nature 359*, 752−4.
40. Gronenborn, A. M., and Clore, G. M. (1993) Identification of the Contact Surface of a Streptococcal Protein G Domain Complexed with a human Fc Fragment. *J. Mol. Biol. 233*, 331−5.
41. Housden, N. G., Harrison, S., Roberts, S. E., Beckingham, J. A., Graille, M., Stura, E. A., and Gore, M. G. (2003) Immunoglobulin-binding domains: Protein L from *Peptostreptococcus magnus*. *Biochem. Soc. Trans. 31*, 716−8.
42. Bogan, A. A., and Thorn, K. S. (1998) Anatomy of Hot Spots in Protein Interfaces. *J. Mol. Biol. 280*, 1−9.
43. Chen, C.-Z., and Shapiro, R. (1997) Site-specific mutagenesis reveals differences in the structural bases for tight binding of RNase inhibitor to angiogenin and RNase A. *Proc. Natl. Acad. Sci. U.S.A. 94*, 1761−6.
44. Lo Conte, L., Chothia, C., and Janin, J. (1999) The atomic structure of protein−protein recognition sites. *J. Mol. Biol. 285*, 2177−98.
45. Koradi, R., Billeter, M., and Wüthrich, K. (1996) MOLMOL: a program for display and analysis of macromolecular structures. *J. Mol. Graphics 14*, 51−5.

BI034873S